MITSUBISHI ELECTRIC RESEARCH LABORATORIES
http://www.merl.com

Propagation Channel Characteristics for Peer-to-Peer Multiple Antenna Systems at 300 MHz

Gunnar Eriksson, Fredrik Tufvesson, Andreas Molisch

TR2006-093 November 2006

Abstract

This paper presents results from the first double-directional measurements of the Multiple-Input Multiple-Output (MIMO) peer-to-peer radio channel in the 300 MHz frequency range. The measurements were performed with vertically polarized circular antenna arrays mounted on cars driving along a route in a semi rural and sub-urban environment. We evaluate the measurements with a high resolution algorithm, thus obtaining a wideband, double-directional characterization of the propagation channel. The delay and directional spread, as well as the small-scale fading statistics are analyzed along the measurement routes and major scatters are identified. The measurements, performed with low antenna heights, show high angular spreads, caused by reflections from trees and buildings and by diffractions over terrain irregularities. We further observe multiple clustes in both the delay and angular domains. The large spreads in these domains indicate a high degree of available diversity, and rich multipath in the considered environment.

IEEE Global Telecommunications Conference (GLOBECOM)

Propagation Channel Characteristics for Peer-to-Peer Multiple Antenna Systems at 300 MHz

Gunnar Eriksson*†, Fredrik Tufvesson†, and Andreas F. Molisch†‡,
*Swedish Defence Research Agency, Box 1165, SE-581 11 Linkoping, Sweden
†Dept. of Electroscience, Lund University, SE-221 00 Lund, Sweden
‡Mitsubishi Electric Research Labs, 201, Broadway, Cambridge, MA 02139, USA
Email: *firstname.lastname*@es.lth.se

***Abstract*— This paper presents results from the first double-directional measurements of the Multiple-Input Multiple-Output (MIMO) peer-to-peer radio channel in the 300 MHz frequency range. The measurements were performed with vertically polarized circular antenna arrays mounted on cars driving along a route in a semi rural and sub-urban environment. We evaluate the measurements with a high resolution algorithm, thus obtaining a wideband, double-directional characterization of the propagation channel. The delay- and directional spread, as well as the small-scale fading statistics are analyzed along the measurement routes and major scatterers are identified. The measurements, performed with low antennas heights, show high angular spreads, caused by reflections from trees and buildings and by diffractions over terrain irregularities. We further observe multiple clusters in both the delay and angular domains. The large spreads in these domains indicate a high degree of available diversity, and rich multipath in the considered environment.**

I. Introduction

Wireless communication systems employing multiple transmit and receive antennas have been shown to offer significantly higher channel capacities compared to single-input single-output systems [1], [2]. For a channel transfer matrix with independent Rayleigh fading entries, the capacity increases linearly with the minimum of the number of transmit and receive antennas. However, in real environments, the achievable capacity depends to a large extent on the radio channel. Therefore, to predict the performance of a MIMO system, it is of highest importance to have accurate channel models. In the development and verification of such models, it is necessary to have input from measurements in relevant environments.

Frequencies in the upper VHF and lower UHF range could be very attractive for mobile military tactical networks and emergency communications. Due to the large wavelength, waves can diffract around obstacles more easily than at higher frequencies; this property is especially important in peer-to-peer networks, where line-of-sight (LOS) exists only rarely. Furthermore, the frequency is high enough to allow terminals with multiple antenna elements, at least for vehicular terminals. It is therefore of high interest to analyze the directional (spatial) properties of the channel and the potential of a MIMO peer-to-peer system operating at frequencies around 300 MHz.

Most of the MIMO measurements in the literature have dealt with the radio channel for mobile or wireless personal communication systems at frequencies around 2 and 5 GHz. Furthermore, most of the measurements are for scenarios involving a base station or an access point. There is only a handful of measurements for MIMO peer-to-peer systems in this microwave range: measurements of angular properties, which are important for MIMO systems, at 1.9 GHz are presented in [3]. Further, analysis of achievable capacities and wideband characteristics for a peer-to-peer MIMO scenario at 2.5 GHz are reported in [4] and [5].

However, the propagation characteristics in the 300 MHz band differ significantly from the microwave band. The size of objects normally seen as very good scatterers, e.g. cars and small buildings, is of the same order as the wavelength. Therefore it is both of theoretical interest and practical interest to measure and characterize the double directional channel in this band.

Yet, to the authors knowledge, there are no double-directional MIMO measurements reported in the literature for frequencies around 300 MHz. Single-input single-output (SISO) measurements are available: wideband measurements of the SISO peer-to-peer radio channel for low antenna heights have been reported in, e.g., [6], whereas measurements for narrowband peer-to-peer scenarios have been performed at 400 MHz for the design and evaluation of the TETRA system [7], [8], and at 225, 450, and 900 MHz for mobile military tactical communication in urban environments [9]. Wideband, high spectral efficient MIMO peer-to-peer communications at 456, 904 and 2177 MHz have been demonstrated in [10].

In this contribution we present results from the first-ever double-directional measurement campaign of the peer-to-peer MIMO wideband outdoor radio channel in the high VHF to low UHF range. We analyze the double-directional characteristics of the channel by considering the joint direction-of-departure (DOD) and direction-of-arrival (DOA). Based on these results we identify important scattering points and propagation mechanisms. We further analyze important channel parameters such as the root mean square (RMS) delay spread and RMS directional spread along the measurement routes. The eigenvalue distribution and capacity of dual antenna arrays operating in those channels are discussed in [11].

The paper is organized as follows. Section II-A describes the measurement scenario. The measurement equipment and the data evaluation is discussed in II-B and II-C, respectively. In Sec. III we present the results from the measurements, and finally in Sec. IV, we conclude this investigation.

1-4244-0357-X/06/$20.00 ©2006 IEEE
This full text paper was peer reviewed at the direction of IEEE Communications Society subject matter experts for publication in the IEEE GLOBECOM 2006 proceedings.

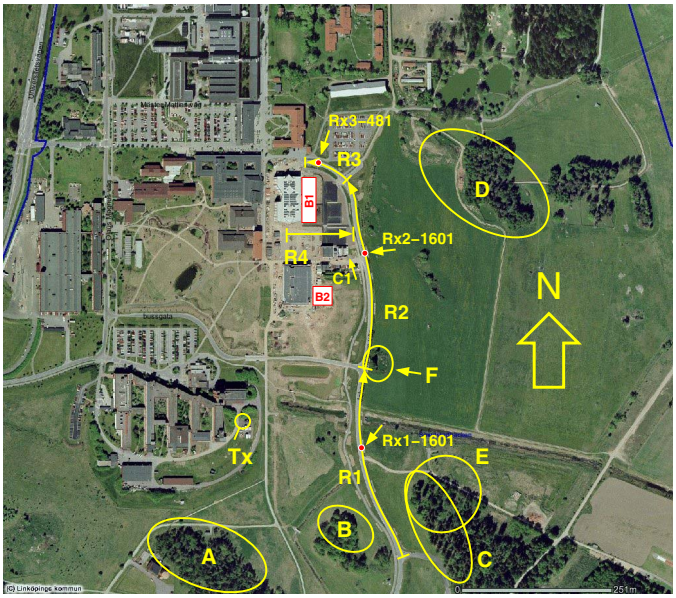

Fig. 1. Aerial photograph of the measurement area.

II. Measurement scenario and data analysis

A. Measurement scenario

The outdoor propagation was measured between terminals with low antenna heights. The transmitter (Tx) and the receiver (Rx) were both placed in cars with the antenna arrays mounted on top of each car. The antenna heights were approximately 1.8 and 2.1 meters above the ground for the Tx and Rx, respectively. The distance between the Tx and Rx ranged from 200 m to 450 m. During the measurements, the Tx was stationary and located approximately 35 m from a large building, while the Rx was driven along four measurement routes. In Fig. 1 the Tx position is marked with a circle labeled Tx and the routes are labeled R1–R4. The driving directions are indicated by arrows.

The routes (i.e., driving distances) have a length of 322, 320, 80, and 111 m, respectively. In the following, when we refer to "distances", we mean driving distances along the route, not distance between Tx and Rx.

Routes 1–3 are all along the south entrance road to the Linköping University campus, while route 4 is located within a parking lot, between some buildings. Two new building, which was not yet present at the time the photograph was taken, are marked with red squares and labeled *B1* and *B2* in Fig. 1. LOS propagation conditions occur in the last part of route 1 and in the first part of route 2. In most of the locations before the LOS part of route 1, the direct path between the Tx and Rx is slightly obstructed by the terrain.

B. Measurement equipment

Measurement data were recorded with a RUSK-LUND channel sounder; the measurement principle is described in [12]. The measurements were performed at a center frequency of 285 MHz and with a bandwidth of 20 MHz. The output power was 43 dBm and the sounding signal was a periodically repeated sequence with a length of 12.8 μs. The guard interval between the repetitions was 12.8μs, which was more than the delay spread in the environment (compare Sec. III-D). The spectrum of the 20 MHz-wide probe signal consisted of 257 frequency lines, spaced 78.125 kHz apart. During post-processing, the channel transfer function was obtained by comparing each frequency line in the measured data with the corresponding lines in data recorded during system calibration.

The Tx and Rx were equipped with identical 8 element antenna arrays. The array is a vertically polarized, 7 element uniform circular dipole array (UCDA), with one additional center element located in an elevated position with respect to the other elements. Additionally, a metallic cylinder, functioning as a reflector, is placed in the center of the UCDA.

The data recording was controlled by trigger pulses from an odometer mounted on one of the wheels. The distance covered between the trigger events was 0.12 m. At each trigger event one data block of 4 channel snapshots (separated by 1.8 ms) was recorded. To increase the signal-to-noise ratio (SNR), the snapshots within each recorded data block were averaged; this implies that the channel is assumed to be approximately stationary over 4 consecutive snapshots. The averaging process increases the SNR by about 6 dB. The noise level was estimated to be corresponding to a transfer function level of -130 dB, which after the SNR enhancement by coherent averaging is about -136 dB; this estimates were obtained by taking differences between consecutive snapshots within the same block.

C. Data analysis

After the first step of post processing, the data from the channel sounder are represented as a series of channel transfer matrices $H_i, i \in [1, I]$, where I is the number of blocks recorded on a route. H_i is of size $n_{\rm rx} \times n_{\rm tx}$, where $n_{\rm rx}$ and $n_{\rm tx}$ is the number of receiver and transmitter antenna elements, respectively. Each element h_{n_1,n_2} of H_i contains the channel frequency transfer function at the 257 measured spectral lines.

The joint angular and delay properties of the measured channel matrices were extracted by using the high resolution SAGE algorithm [13]. Thus, each H is described by a signal model with a finite number of multi-path components (MPC) so that

$$h_{n_1,n_2}(k, \alpha_l, \tau_l, \phi_l^{\rm rx}, \phi_l^{\rm tx}) = \sum_{l=1}^{L} \alpha_l e^{j2\pi\Delta f \tau_l k} G_{\rm rx}(n_1, \phi_l^{\rm rx})\, G_{\rm tx}(n_2, \phi_l^{\rm tx}), \quad (1)$$

where L is the number of MPC, Δf the spacing between the frequency sub channels, $\alpha_l, \tau_l, \phi_l^{\rm rx}$, and $\phi_l^{\rm tx}$ are the complex amplitude, delay, angle of arrival, and angle of departure, respectively, of the l:th MPC. Furthermore, $k, n_1, n_2, G_{\rm rx}$, and $G_{\rm tx}$, are frequency sub-channel index, receiver element index, transmitter element index, receive antenna response, and transmit antenna response, respectively. For the SAGE evaluations, only the 7 circularly placed elements of the antenna array were used.

1-4244-0357-X/06/$20.00 ©2006 IEEE
This full text paper was peer reviewed at the direction of IEEE Communications Society subject matter experts for publication in the IEEE GLOBECOM 2006 proceedings.

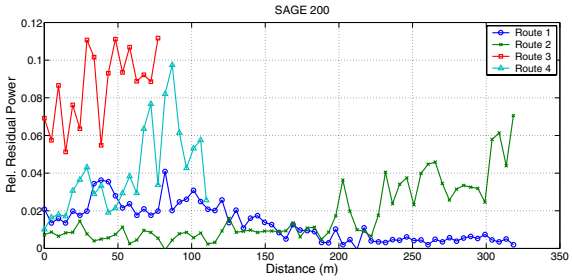

Fig. 2. Relative power residual for 200 SAGE components vs. driving distance along the four routes.

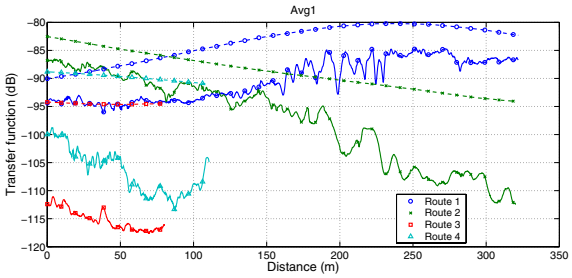

Fig. 3. Mean channel transfer functions vs. distance along the routes. The solid lines are directly measured values and the dashed lines are from the flat earth model.

D. Power extracted by the SAGE algorithm

An important test for the validity of the underlying data model is to check how much of the totally received power can be described by the MPCs of Eq. (1). The amount of captured power depends on L, as well on the propagation environment. A more complex environment would need more MPCs to capture a given fraction of the total power. In case of diffuse scattering, or some other mismatch in the signal model (e.g. spherical waves or components not arriving in the horizontal plane), the number of required components can be very high. An estimate of the relative power residual, i.e. the amount of power not captured by SAGE, as a function of the number of extracted MPCs L, is given as

$$\Lambda(L) = \frac{\|H_{\text{meas}}\|_F^2 - \|\widehat{H}(L)\|_F^2 - P_{\text{noise}}}{\|H_{\text{meas}}\|_F^2}, \qquad (2)$$

where $\|\cdot\|_F$ is the Frobenius norm, H_{meas} the measured channel matrix, $\widehat{H}(L)$ the reconstructed channel matrix obtained from the signal model (1) and with the parameters taken from the SAGE estimates, and P_{noise} is the estimated noise power obtained from the direct measurements. The noise power is estimated from the upper part of the power delay profile ($8 - 10$ μs), where no signal components were observed in this scenario. Hence, the estimated noise power is assumed to be statistically independent of the signal power.

In our data analysis, SAGE was run for a fixed, predefined, number of components L at each analyzed position. The SAGE runs were repeated for different values of the parameter L; Fig. 2 shows $\Lambda(L)$ for $L = 200$. For the measurements on route 1 and 2 the power residual is very low. Most of the positions have a Λ of only a few percent for $L \geq 150$. However, at the end of route 2, Λ starts to increase. The first part of route 4 shows a fairly low power residual, but at about 70 and 85 m along the route there are two larger peaks. At these positions the received power is about the lowest on the route. Route 3 shows a rather high power residual; and again, the residuals are largest where the pathloss is largest.

III. Results

A. Propagation loss

The mean transfer function between the transmitter and receiver was calculated by averaging the received power over all frequency sub-channels, and over all combinations of transmitter and receiver antenna elements. In Fig. 3 the measured transfer function is shown together with the transfer function obtained from a flat-earth (two-ray) propagation model[1] whose propagation loss is [14]

$$L_{\text{FE}} \approx \left(\frac{d^2}{h_{\text{tx}} h_{\text{rx}}}\right)^2, \qquad (3)$$

where d is the propagation distance, h_{tx} and h_{rx}, the transmitter and receiver antenna height, respectively. The general behavior of the measured and modeled transfer functions are rather similar for route 1. The differences are largest between 100–200 m, which corresponds to the part where the LOS is obstructed by a small hill between the transmitter and receiver. For route 2 the difference between the measured and modeled transmission loss starts to increase significantly at about 150–200 m, indicating that the direct path starts to be shadowed. On route 3 and 4, which are completely in non-LOS (NLOS) conditions, there are substantial differences between the measurements and the model.

B. Dominant propagation mechanisms

From the extracted double-directional description of the channel we will here explain some of the observed propagation mechanisms for a few typical receiver positions along the routes. This will give an idea of the dominant propagation mechanisms in the environment. Fig. 4 and 5 show the DOA-DOD plots of the MPC components; each MPC is shown as a circle whose center corresponds to the nominal DOAs and DODs. The delay of the MPCs is color-coded; the powers are indicated by the size of the circles.

1) Route 1: Fig. 4(a) shows the MPCs at the starting position of Route 1. We see that some components have a DOD around -45 degrees, i.e., close to the LOS direction. Others have a DOD around 135 degrees; those MPCs undergo a double-reflection at a part of the building that acts as like a corner reflector. It is remarkable that the strongest MPC (large circle in cluster S_1) is one that undergoes this double-reflection. We also note that the area marked *C* in Fig. 1 leads to significant reflections, and gives rise to the MPCs with a DOA between -30 and -150 degrees (clusters S_3–S_5).

[1]Note that the well-known Okumura-Hata model can not be used, because the "base station" height is outside the range of validity for this model.

1-4244-0357-X/06/$20.00 ©2006 IEEE
This full text paper was peer reviewed at the direction of IEEE Communications Society subject matter experts for publication in the IEEE GLOBECOM 2006 proceedings.

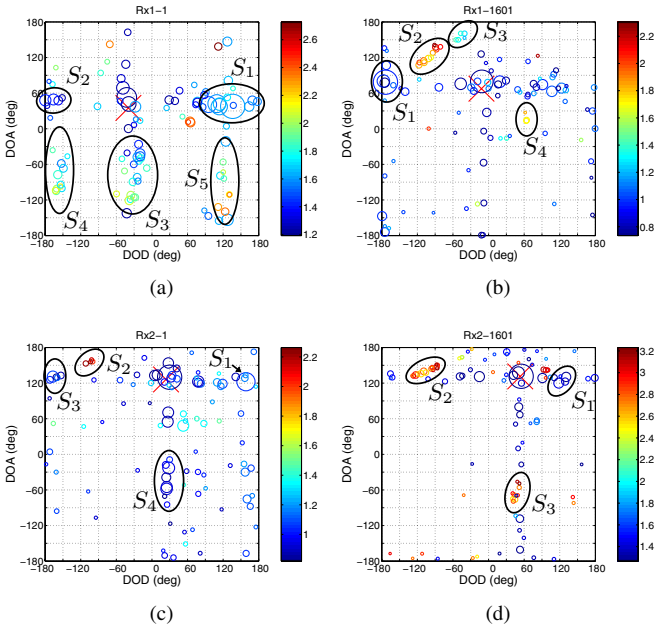

Fig. 4. Joint DOA-DOD at four LOS (or near LOS) positions. The area of the circles are proportional to the amplitude and normalized to the strongest component. The color indicates the delay in μs.

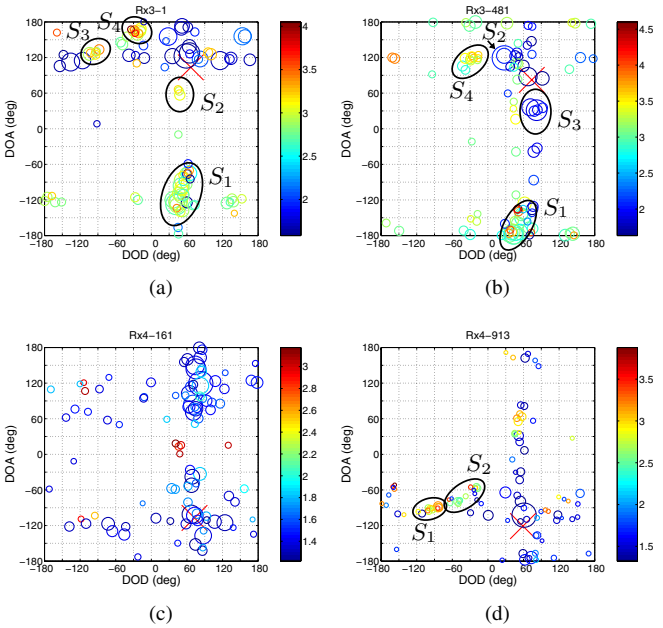

Fig. 5. Joint DOA-DOD at four NLOS positions. The area of the circles are proportional to the amplitude and normalized to the strongest component. The color indicates the delay in μs.

In Fig. 4(b) the propagated components for position Rx1-1601, located 193 m from start of route 1, are shown. At this position the LOS is obstructed by the terrain. Again a reflected component S_1 is of the same magnitude as the quasi-LOS component at the *X* marker. The signals in the clusters S_2 and S_3 come from reflections within area *A* and *B* in Fig 1, respectively.

2) Route 2: On the first part of this route we have LOS conditions but at a position 200 m from the start we pass a building and the rest of the route is NLOS. In Fig. 4(c) the MPCs at the starting position of route 1 are shown. The LOS component at the *X* marker is the strongest component. Wall reflections in the building close to the transmitter give rise to the components marked S_1 and S_3. The MPCs in cluster S_2, with a delay of about 1.3 μs relative to the LOS component, are due to reflections in the trees within area *A* in Fig. 1. Furthermore, we have a cluster S_4 with MPCs from reflections in trees close to the receiver (area *F* in Fig. 1). Fig. 4(d) shows the MPCs at position Rx2-1601 (193 m from start). The components from reflections in area *A* are here still present in cluster S_2. The MPCs in S_3 come from area *D* in Fig. 1.

3) Route 3: This route is located deep into the shadow region. Signal components propagating into positions along this route must be diffracted around obstacles or reflected by other objects. From the joint DOD-DOA angles in Fig. 5(a) we can identify some of the propagation mechanisms into the starting position on route 3. Firstly, we see a large group of components propagating close to the quasi-LOS direction (marked with a red *X*). The different components take slightly different paths; some have diffracted over rooftops, others around building corners etc. As a consequence, this group of MPCs has a rather high spread in DOA (and to some extent also in DOD). Secondly, we have a large cluster (S_1) of components with DOA angles between -90 and -140 degrees and a delay of about 1μs relative to the first arriving MPCs. This cluster is caused by reflections in the trees within the area marked with a *D* in Fig. 1. Signals reflected within area *D* are then also reflected in the building *B1* and causing the components marked S_2. Furthermore, clusters S_3 and S_4 have been identified as coming from area *A* and *E*, respectively.

In Fig. 5(b) the DOD-DOA are shown for a position 58 m from the start of route 3. At this position the LOS direction is completely blocked by a building close to the receiver. We observe two MPCs relatively close to the LOS direction (*X*), probably caused by over-the-rooftop diffraction. However, the strongest contributions come from the cluster S_2, which is caused by a reflection in some trees at the position marked *F* in Fig. 1, and S_3, which are signals that have traveled in a direction slightly more to the north than the LOS direction, and then reflected, or diffracted, into the receiver from the west. The components from the area *D* in Fig. 1 are still present at S_1. The MPCs in the cluster marked *S4* comes from scatter regions *B* and *E*.

4) Route 4: This route is also located deep in the shadow region. Fig. 5(c) shows the DOD-DOA plot at a position 20 m from the start of this route. We have here a dominant DOD. The DOAs are widely spread out; however, in the directions around -100 and $+90$ degrees, more MPCs occur, and they have higher power. The peak at -100 degrees is close to the LOS direction, while the direction of +90 degrees corresponds to reflections in a building at the opposite direction. There might be several reasons for the large spread in DOA. Firstly,

1-4244-0357-X/06/$20.00 ©2006 IEEE
This full text paper was peer reviewed at the direction of IEEE Communications Society subject matter experts for publication in the IEEE GLOBECOM 2006 proceedings.

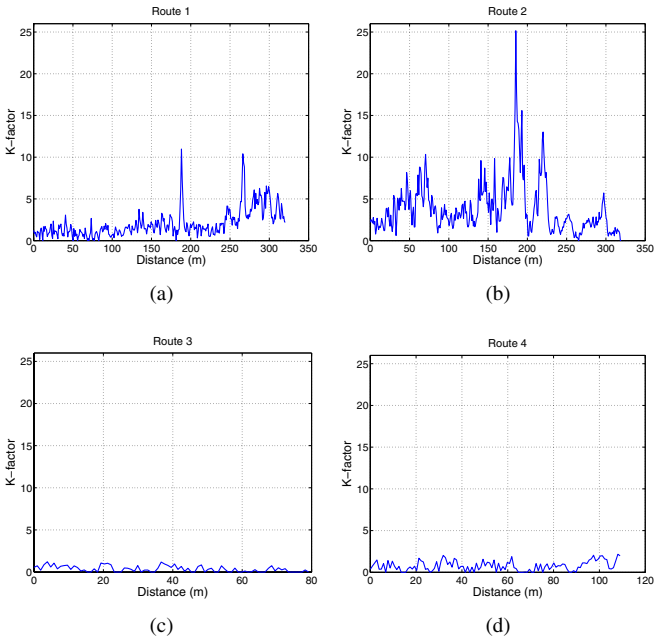

Fig. 6. Estimated Ricean K-factor along the routes 1–4.

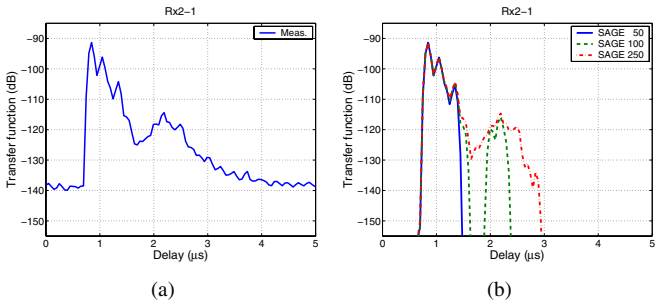

Fig. 7. PDP at the start of route 2. (a) Measured profile. (b) PDP from reconstructed channel matrices with 50, 100, and 250 SAGE components.

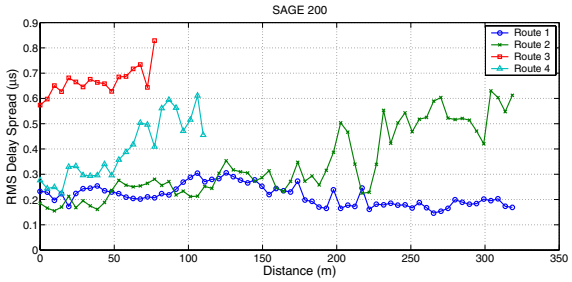

Fig. 8. RMS delay spread vs. driving distance along the four routes.

the diffracted paths, MPCs that are diffracted over the rooftop of the building to the south, might have split into a number of paths due to scattering objects on the roof. Secondly, the receiver is located within a parking lot with a lot of objects that might cause local scattering. Finally, due to the rooftop diffraction, the diffracted signal arrives at quite an elevated angle, which might cause a mismatch in the signal model.

At the end of this route (Fig. 5(d)), the propagation conditions have completely changed. Here, we have a single dominating component, which is diffracted around the corner *C1* (Fig. 1). The cluster S_1 originates from reflections in region *A* and the cluster S_2 comes from the regions *B* and *C*.

C. Fading

We next investigate the small-scale fading statistics for the propagation between the two (horizontally omnidirectional) center elements of the array. Following the standard modeling assumptions, we describe the fading as Rician (of which Rayleigh fading is a special case) and extract the Rician K-factor according to the method of Greenstein et al. [15]. Fig. 6 shows the obtained Rice factor, when extracted from 8 consecutive blocks. It is noteworthy that even for the LOS situations (second part of route 1, and first part of route 2), the K-factor rarely exceeds 7.

D. Delay properties

The impulse responses were computed by a discrete inverse Fourier transformation of the complex frequency transfer functions. To reduce the side-lobe levels, a Blackman window was applied on the frequency data before the transformation. The power delay profile (PDP) was computed by averaging the squared magnitudes of the channel impulse responses over all spatial channels (channels from each Tx element to each Rx element) within a block H_i. In Fig. 7(a) the PDP at the starting position of route 2 is presented. The PDP shows two distinct peaks, separated by approximately 2 μs. The second peak is about 20 dB weaker than the first one. It is also interesting to compute the PDP from the MPCs extracted by the SAGE algorithm. Fig. 7(b) shows such PDPs from reconstructed channel matrices with a different number of components (note that this is equivalent to a bandlimited filtering of the discrete impulse response obtained from SAGE). From this plot it can be seen how the approximation by the reconstructed PDP improves as the number of considered MPCs increases.

A commonly used measure characterizing the PDP is the RMS delay spread. It is defined as the square root of the second central moment of the PDP [14]. The RMS delay spreads for the measured routes are given in Fig. 8. Along route 1 the delay spread is fairly constant with values at about 0.15–0.3 μs. On route 2 there is an increase in the spread from about 0.2 μs in the beginning to about 0.6 μs at the end of the route. The spread on route 3 shows no general trend but varies between 0.6–0.8 μs. For route 4 there is again a trend of increasing spread along the route, starting at 0.3 μs and ending at about 0.7 μs. We can see that for larger propagation loss, the delay spread is larger, which is consistent with the observations of Greenstein et al. [16]. The delay spread observed in this investigation is slightly less than what has been reported for the 2.5 GHz rural peer-to-peer scenario in [5]. The propagation distance were, however, larger for many of the links in the latter investigation.

1-4244-0357-X/06/$20.00 ©2006 IEEE
This full text paper was peer reviewed at the direction of IEEE Communications Society subject matter experts for publication in the IEEE GLOBECOM 2006 proceedings.

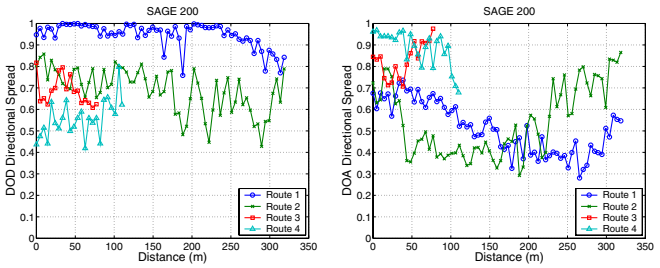

(a) DOD (b) DOA

Fig. 9. Directional spread vs. driving distance along the routes.

E. Directional properties

The directional properties of the radio channel can be characterized by the RMS directional spread σ_Ω [17]. It is the square root of the second central moment of the directional vector Ω. If the impulse response consists of discrete components (as is the case for the SAGE model) and all the waves are incident in the horizontal plane, then [17], [14]

$$\sigma_\Omega = \sqrt{\sum_l |e^{j\phi_l} - \mu_\Omega|^2 P(\phi_l)}, \qquad (4)$$

where $\mu_\Omega = \sum_l e^{j\phi_l} P(\phi_l)$, and $P(\phi_l)$ is the angular power spectrum normalized as $\sum_l P(\phi_l) = 1$. Fig. 9 presents the result of the directional spread of DODs and DOAs for the measured routes. Along route 1 the spread of the DOD is very large, namely close to 1 for a large part of the route. The cause of the high spread is probably strong reflections in the buildings behind the transmitter, so that the strongest signal components are at directions differing 180 degrees. The spread in DOA starts at about 0.7 and decreases as the receiver moves closer to the transmitter and has its lowest value of 0.3–0.4 when it is at the closest position, and then there is an increase in spread again. Route 3 has a spread in DOD of 0.6–0.8 and in DOA of 0.7–0.95. The DOD spread at route 4 is lower than for the other routes because there is no efficient reflector "behind" the transmitter, where "behind" means 180° offset from the quasi-LOS direction. The high DOA spread on this route is caused by reflections between the buildings on each side of the receiver.

IV. Conclusions

We presented results from the first ever double-directional measurements of MIMO peer-to-peer propagation channels in the 300 MHz range. This frequency range and application scenario is of great importance to military communications, as well as direct-mode trunk radio and emergency communications. We evaluated the measurements with a high resolution algorithm, thus obtaining a wideband, double-directional characterization of the propagation channel (i.e., delay, DOA, and DOD of the MPCs). Due to the low height of the transmitter as well as the receiver, reflections from trees, diffractions over terrain irregularities etc. are important, so that directional spreads are high. We observed multiple clusters in the delay as well as in the angular domains. The large spreads in all of these domains indicate a high degree of available diversity, and the possibility for effective spatial multiplexing. Future work will concentrate on the statistical modeling of the measurements, and an evaluation of the impact on system design.

V. Acknowledgment

We thank Bengt Lundborg and Åsa Waern for helpful discussions, and their support and encouragement. The help of Mikael Alexandersson and Elisabeth Löfsved in calibrating the antenna arrays is gratefully acknowledged.

References

[1] J. H. Winters, "On the capacity of radio communications systems with diversity in rayleigh fading environments," *IEEE J. Select. Areas Commun.*, vol. 5, pp. 871–878, 1997.

[2] G. J. Foschini and M. J. Gans, "On limits of wireless communications in a fading environment when using multiple antennas," *Wireless Personal Commun.*, vol. 6, pp. 311–335, 1998.

[3] G. D. Durgin, V. Kukshya, and T. S. Rappaport, "Wideband measurements of angle and delay dispersion for outdoor and indoor peer-to-peer radio channels at 1920 MHz," *IEEE Trans. Antennas and Propagat.*, vol. 51, no. 5, pp. 936–944, May 2003.

[4] D. Chizhik, J. Ling, D. Samardzija, and R. A. Valenzuela, "Spatial and polarization characterization of MIMO channels in rural environment," in *Proc. 61st IEEE Veh. Technol. Conf. (VTC '05 Spring)*, vol. 1, Stockholm, Sweden, May 2005, pp. 161–164.

[5] J. Ling, D. Chizhik, D. Samardzija, and R. A. Valenzuela, "Wideband and MIMO measurements in wooded and open areas," in *Proc. IEEE AP-S Int. Symp.*, vol. 3B, Washington, USA, July 2005, pp. 422–425.

[6] C. Hendrickson and C. Yerkes, "Wideband wireless peer to peer propagation measurements," in *Thirty-Third Asilomar Conference on Signals, Systems, and Computers*, vol. 1, 1999, pp. 183–189.

[7] "ETS 300 396-2: Trans-European Trunked Radio (TETRA); Technical Requirements for Direct Mode Operation (DMO) — Part 2: Radio Aspects," European Telecommunication Standards, Tech. Rep., 1999.

[8] I. Z. Kovács, P. C. F. Eggers, K. Olesen, and L. G. Petersen, "Radio channel description and quality of service for TETRA direct mode operation in forest environments," in *Proc. 54th IEEE Veh. Technol. Conf.*, Atlantic City, USA, Sept. 2001, pp. 1970–1974.

[9] J. R. Hampton, N. M. Merheb, W. L. Lain, D. E. Paunil, R. M. Shuford, and W. T. Kasch, "Urban propagation measurements for ground based communication in the military UHF band," *IEEE Trans. Antennas and Propagat.*, vol. 54, no. 2, pp. 644–654, Feb. 2006.

[10] J. C. Liberti, J. C. Koshy, T. R. Hoerning, C. C. Martin, J. L. Dixon, A. A. Triolo, R. R. Murray, and T. G. McGiffen, "Experimental results using a MIMO test bed for wideband, high spectral efficiency tactical communications," in *Proc. MILCOM 2005*, Oct. 2005.

[11] G. Eriksson, F. Tufvesson, and A. F. Molisch, "Potential for MIMO systems at 300 MHz — Measurements and analysis," in *Proc. Antenn 06*, Linkoping, Sweden, May 2006, to be published.

[12] R. S. Thomä, D. Hampicke, A. Richter, G. Sommerkorn, and U. Trautwein, "MIMO vector channel sounder measurement for smart antenna system evaluation," *European Transactions on Telecommunications*, vol. 12, no. 5, pp. 427–438, Sep./Oct. 2001.

[13] B. H. Fleury, P. Jourdan, and A. Stucki, "High-resolution channel parameter estimation for MIMO applications using the SAGE algorithm," in *Proc. 2002 Int. Zurich Seminar on Broadband Communications—Access, Transmission, Networking*, ETH Zurich, Switzerland, Feb. 2002, pp. 30–1–30–9.

[14] A. F. Molisch, *Wireless Communications*. IEEE Press – Wiley, 2005.

[15] L. J. Greenstein, D. G. Michelson, and V. Erceg, "Moment-method estimation of the Ricean K-factor," *IEEE Communications Letters*, vol. 3, no. 6, pp. 175–176, June 1999.

[16] L. J. Greenstein, V. Erceg, Y. S. Yey, and M. V. Clark, "A new path-gain/delay-spread propagation model for digital cellular channels," *IEEE Trans. Veh. Technol.*, vol. 46, no. 2, pp. 477–485, May 1997.

[17] B. H. Fleury, "First- and second-order characterization of direction dispersion and space selectivity in the radio channel," *IEEE Trans. Inform. Theory*, vol. 46, no. 6, pp. 2027–2044, Sept. 2000.

1-4244-0357-X/06/$20.00 ©2006 IEEE

This full text paper was peer reviewed at the direction of IEEE Communications Society subject matter experts for publication in the IEEE GLOBECOM 2006 proceedings.